ELSEVIER

Contents lists available at ScienceDirect

Computers and Chemical Engineering

journal homepage: www.elsevier.com/locate/compchemeng





Process integration and systems optimization for the hydrodeoxygenation of 5-hydroxymethylfurfural to dimethylfuran

Zhaoxing Wang ^{a,b,1}, Yuqing Luo ^{a,1}, Prahalad Srinivasan ^a, Yifan Wang ^{a,b}, Tai-Ying Chen ^{a,b}, Marianthi G. Ierapetritou ^{a,*}, Dionisios G. Vlachos ^{a,b}

- a Department of Chemical and Biomolecular Engineering, University of Delaware, 151 Academy St., Newark, DE 19716, United States
- b Catalysis Center for Energy Innovation, RAPID Manufacturing Institute, and Delaware Energy Institute (DEI), University of Delaware, 221 Academy St., Newark, DE 19716, United States

ARTICLE INFO

Keywords: Process integration Feedstock purity TEA LCA Active learning CO₂ emissions

ABSTRACT

Most biomass reaction studies have focused on optimizing product yield without considering cost and emissions as key metrics; they consider pure feeds without accounting for process integration resulting from separation and recycling and often change one parameter at a time to maximize yield. Here, we propose a framework to overcome the above issues. We demonstrate it for the hydrodeoxygenation (HDO) of 5-hydroxymethylfurfural (HMF) to produce 2,5-dimethylfuran (DMF), a crucial reaction in making lignocellulosic biomass-based platform chemicals. We consider the impact of water in the feed stemming from the sugar dehydration reactor on the HDO in 2-pentanol over a Ru/C catalyst, guided by an active learning experimental design (NEXTorch toolkit), combined with Aspen Plus process flowsheet simulation, techno-economic analysis and life cycle assessment. We demonstrate that Bayesian optimization of process flowsheets significantly reduces production costs by 26% and greenhouse gas emissions by 15% after striking a balance between raw material usage, solvent loss, and utility consumption. Such reductions are strongly correlated to the product yield due to the dominant cost of the feed. Interestingly, a slight amount of water negatively impacts greenhouse gas emissions more than production costs, requiring relatively high purity in process integration.

1. Introduction

Lignocellulosic biorefineries can reduce petrochemical reliance and combat climate change. Various pathways for lignocellulosic biomass valorization have been investigated, and platform chemicals have been identified. Among them, 5-hydroxymethylfurfural (HMF) is a "top-10" platform chemical (Bozell and Petersen, 2010; van Putten et al., 2013). It is produced *via* hexose dehydration, where three atomic oxygens are removed as water molecules in an aqueous phase. Downstream utilization of HMF for most applications requires further oxygen removal. 2, 5-dimethylfuran (DMF) is a critical HMF-derived intermediate for producing alternatives to petroleum-derived chemical building blocks (Nakagawa et al., 2013). DMF is produced via the hydrodeoxygenation (HDO) of HMF (Jae et al., 2014, 2013; Wijaya et al., 2015). Process integration requires feeding the product from one process to the next and requires separations and purification, as a downstream process may experience catalyst poisoning and undesirable reaction pathways.

Cascading processes can benefit from a knowledge of process integration.

Water is present in HMF and DMF production processes as a solvent in fructose dehydration and as a product in HMF HDO (Fig. 1). In the dehydration process, an organic phase is often also used to extract HMF to avoid its further degradation through rehydration or condensation reactions (Esteban et al., 2020; van Putten et al., 2013). An often overlooked effect is that the solubility of water in high-performing HMF extraction solvents at reaction temperatures is large (Wang et al., 2020). For example, the water solubility in pentanol is as high as 35 wt% at reaction temperatures. The effects of water on HDO include direct participation in the reaction (e.g., on transition state stabilization), catalyst site blocking, catalyst modification, etc (Gilcher et al., 2022; Zhang and Li, 2022). Akpa et al. (2012) investigated the role of water in 2-butanone hydrogenation over Ru/SiO₂, revealing that water facilitates the formation of certain intermediates via proton shuttling, without always lowering the activation barriers for all reaction steps. Zhao et al.

^{*} Corresponding author.

 $[\]textit{E-mail address:} \ \, \underline{\mathsf{mgi@udel.edu}} \ \, (M.G. \ \, \mathrm{Ierapetritou}).$

¹ These authors contributed equally to this work.

reported an increase in the yield of hydrogenated products of furfural over Pd/Al₂O₃ when cyclohexane solvent was replaced with water. This behavior was attributed to water-mediated proton transfer that assists in reducing the activation barrier for hydrogenation of the carbonyl group (Zhao et al., 2019). Gilcher et al. studied the hydrogenation of hydroxyl-α-angelicalactone (HAH) using Ru catalysts and found that a 1:1 molar ratio of water to isopropanol (IPA) maximizes the conversion to the desired product. Exceeding this water ratio reduces efficacy, and while low water levels boost furan hydrogenation, high levels cause significant carbon loss, potentially due to byproduct formation.¹⁰ For HMF HDO, high concentrations of water may decrease the reaction rate. However, separating water can be expensive and energy consuming due to its high heat of vaporization, and biomass intermediates are often thermally unstable. Design decisions should thus rely on experiment-driven comprehensive techno-economic analysis (TEA) and life cycle assessment (LCA) to develop water mitigation strategies.

In this work, we assess the water effects on process integration of the HMF HDO reaction with the fructose dehydration. We present a framework that integrates lab bench-scale experiments, active learning, TEA, and LCA to maximize HMF conversion and DMF selectivity, as conventionally done, and minimize the economic and environmental footprint. Specifically, we employ NEXTorch (Next EXperiment toolkit in PyTorch) (Chen et al., 2020; Ebikade et al., 2020; Wang et al., 2021a) to find optimal operating conditions and accelerate flowsheet design and optimization.

2. Materials and methods

2.1. Materials

5-hydroxymethyl furfural (Sigma-Aldrich W501808, \geq 99%), 2,5-dimethylfuran (Sigma-Aldrich 177,717, 99%), 2-pentanol (Sigma-Aldrich W331600, \geq 98%), 2-propanol (Fisher Scientific A464–4, \geq 99.9%), ruthenium on carbon (Sigma-Aldrich 206,180, 5 wt% loading, lot #MKBZ2792V), ASTM-Type 1 water (Millipore Direct-Q 3 UV), nitrogen (Keen Compressed Gas Co., Grade 5.0), and hydrogen (Matheson, UHP grade) were used in this work.

2.2. Experimental design space and optimization

Fig. 2 shows the workflow for Bayesian optimization in two stages. The focus of stage 1 was to use Bayesian optimization and suggest experimental conditions that improve reaction conversion and selectivity. A design space was created spanning five factors, reaction time (h), HMF feed concentration (wt%), water feed concentration (wt%), reaction temperature (°C), and hydrogen partial pressure (bar). The Minitab (Minitab, LLC) generated a 2⁵⁻¹ factorial design with duplicates (16 conditions) to collect data at the corners. For probing the internal space, a 15-point Latin hypercube (LHC) design was initially generated (Wang et al., 2021a). Five Bayesian optimization trials, each of three individual runs were added using NEXTorch. The Monte Carlo q-expected improvement (qEI) acquisition function in NEXTorch was used to suggest the next trial. For each trial, up to six candidate experimental conditions were suggested, and three distinct conditions were selected for experiments in three identical reactors. After reaching optimal reaction conditions, the data points collected in each iteration were regressed to provide HMF conversion and DMF selectivity surrogate models. Finally, stage 2 of the Bayesian optimization aimed to find reaction conditions with minimum production costs or emissions based on the aforementioned reaction regression model and process flowsheet simulation.

2.3. HDO experiments

In a typical reaction, a 50 mL Parr 4790 pressure vessel was charged with 5 wt% fresh-from-bottle Ru/C catalyst at 35:1 HMF:Ru ratio, 30 mL of a secondary alcohol, and the corresponding quantities of water and HMF. For all reaction mixtures, the catalyst, water, and HMF weights were calculated assuming that the final mixture has the density of 2-pentanol, regardless of their composition. The reactor was then sealed and nitrogen-purged three times and charged with sufficient nitrogen to reach 20 barg total headspace pressure. The headspace was then filled with the prescribed pressure of hydrogen. The reactor was heated with a PID-controlled band heater, reaching the prescribed temperature typically within 20 min, while magnetically stirred at 300 rpm. The reactor

Fig. 1. Reaction network of HMF over Ru/C in 2-pentanol.

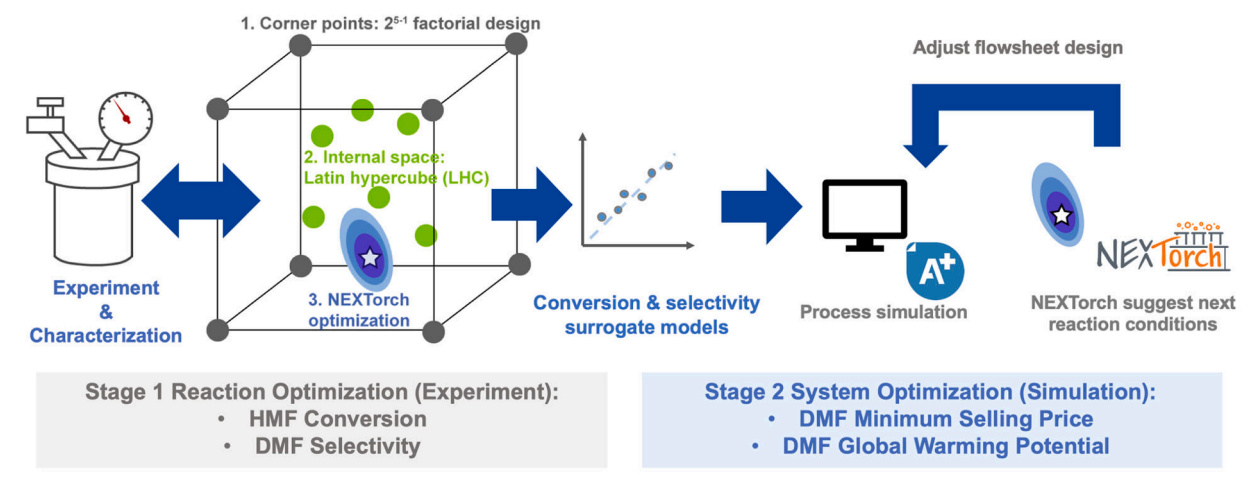


Fig. 2. Workflow of the two-stage process integration and systems optimization based on Bayesian optimization.

was quenched in an ice bath after holding at the reaction temperature for a specified time. The reactor contents were then collected and filtered for quantification. For high concentrations of water, the entire post-reaction mixture was extracted and centrifuged at 5000 g for 1 min. When a biphasic system was found after centrifugation, the aqueous and organic phase volumes were recorded, and both phases were separately extracted and filtered for GC characterization. For these runs, the DMF selectivity and HMF conversion were calculated for the entire biphasic system.

2.4. Product quantification

An Agilent 7890B gas chromatograph (GC) was used with a flame ionization detector (FID) and an HP-INNOWax column (30 $m\times0.25$ mm, 0.25 µm, Agilent 19091N-133I) for product quantification. External calibration curves were created for HMF and DMF for the relevant concentration ranges. For furanic species in the reaction network without attainable concentration standards, the calibration curve of HMF was used instead. These species were identified using a Shimadzu GC-2010 gas chromatograph coupled with an INNOWax column of identical specifications and a Shimadzu GCMS-QP2010 Plus gas chromatograph-mass spectrometer. The standard deviation in HMF conversion and DMF selectivity was $\sim\!1\%$.

For water-in-2-pentanol solubility estimates, the organic phase samples' water content was quantified using a Mettler Toledo V20 Karl Fischer titrator, with the Honeywell Fluka Composite 5 titrant and Honeywell Fluka Methanol Dry titration medium. The titrant concentration was calibrated with ASTM Type 1 water (Millipore Direct-Q 3 UV). Detailed *in situ* sampling procedures for water-in-organic solubility meassurements can be found in our previous works (Wang et al., 2020, 2021b).

2.5. Process simulation of representative HDO reaction conditions

Five representative HDO reaction conditions were selected from the stage 1 reaction optimization for initial flowsheet simulation, TEA, and LCA in Aspen Plus v11 (Table 1).

 $\begin{tabular}{ll} \textbf{Table 1} \\ \textbf{Reaction conditions used for initial Aspen Plus process flowsheets.} \\ \end{tabular}$

Case #	Temp (°C)	Water (wt.%)	HMF (wt.%)	Time (h)	H ₂ Pressure (bar)	DMF select (%)	HMF conv (%)	Sample method
I	190	20	1	6	10	68.5	100	Factorial
II	190	20	5	6	0	46.5	100	Factorial
III	210	0	5	3	10	44.7	70.9	Factorial
IV	203	1	1	3	9	77.2	100	LHC
V	195	0	1	4.6	10	79.2	100	qEI

The universal quasi-chemical activity coefficient (UNIQUAC) model was chosen for the liquid-vapor and liquid-liquid phase behavior (Abrams and Prausnitz, 1975). Due to the pentanol/water azeotrope and vastly different feedstock compositions, four different flowsheet configurations were designed for product separation. The flowsheet of reaction condition case I is shown in Fig. 3, while the rest could be found in the Supplementary Material.

The hydrogen gas and HMF solution were pressurized and heated to the reaction condition before sending to R-1. After the HDO reaction, flash drum F-1 cooled down the system to 65 °C and recycled the hydrogen gas. Then, humins were removed by filtration. It was assumed in the base case that most of the liquid phase was retained with 1% loss in the waste humins stream. Future improvement on the filtration system may reduce the solvent makeup, and its impact on the production cost was evaluated through the sensitivity analysis (Fig. 8B). The liquid stream was sent to two distillation columns in series, the first one of which (C-1) recycled most of the pentanol solvent. The second column (C-2) separated nearly all pentanol as the pentanol/water azeotrope, leaving DMF mixed with water in the bottom. Two decanters cooled down both the bottom (D-1) and distillate streams (D-2) to 40 °C, so that excess water was removed by phase separation. The process capacity was chosen as 10,000 kg HMF/h (80,000 t/year), which was in line with the scale considered in a recent paper that produced HMF as an intermediate (Chang et al., 2020).

2.6. Process techno-economic analysis and life cycle assessment

The Aspen Process Economic Analyzer V11 was used to calculate the capital and operating costs (Aspen Economic Analyzer V11, 2019). The minimum selling price (MSP), the selling price of the product when the net present value is zero at the end of the recovery period, was determined through discounted cash flow analysis for each condition (Athaley et al., 2019b). A 15% internal rate of return (ROR) on investment and a 35% corporate tax were assumed (Luo et al., 2022). The straight-line method for depreciation with 10% salvage value after 20 years was applied (O'Dea et al., 2022). The catalyst cost for the HDO reaction was estimated as the precious metal cost plus \$11/kg for the supported

Recycled Solvent HMF Pentanol Water P-1 Recycled Solvent Recycled Solvent

Fig. 3. Hydrodeoxygenation process flowsheet under reaction condition case I (190 °C, 10 bar H₂, 20 wt% water, 1 wt% HMF loading, and 6 h reaction time).

catalyst manufacturing (Kazi et al., 2011). The unit price of ruthenium used in the Ru/C catalyst was \$6430/kg (BASF, 2024). The catalyst was replaced every six months, and the catalyst manufacturer could recover 99% of the precious metal in the spent catalyst. Hydrogen's price was assumed \$1570/t (Kuznetsov et al., 2020). The price of water was \$0.5/t and the purchase price of quicklime was \$120/t when the water vapor in the recycled hydrogen gas needed to be removed (U.S. Geological Survey, 2016). The biomass-based HMF cost was estimated to be as low as \$0.88/kg (Kazi et al., 2011). The solvent, pentanol, was mainly synthesized by oxo synthesis, the price of which was assumed to be similar to general oxo alcohols (e.g., butanol) at around \$1500/t (Peter Lappe and Hofmann, 2011).

A "cradle-to-gate" system boundary for LCA was defined, which considers the upstream raw material (e.g., HMF (Athaley et al., 2019a; Luo and Ierapetritou, 2020)) extraction, utility generation, and the DMF production stages (Fig. S11). The functional unit is chosen as 1 kg of DMF produced by the HDO reaction. Because quantifying greenhouse gas emissions has attracted growing attention for its essential role in renewable technology development and policy making, the global warming potential (GWP) was selected for the environmental impact evaluation (Zheng and Suh, 2019). It is assumed that only 1% of the cooling water is lost during the operation while most of it could be reused (Athaley et al., 2019a). The Ecoinvent v3.7 database was used to provide the background emission data (Wernet et al., 2016), and the Tool for the Reduction and Assessment of Chemical and other environmental Impacts (TRACI) method was selected for the impact assessment (Bare, 2011).

2.7. Flowsheet Bayesian optimization

Bayesian optimization of the process flowsheet follows the experimental work. After the first stage of reaction conversion and selectivity maximization (Fig. 2), 46 data points (Table S1) were collected to perform regression (Figs. S1 and 2). An ordinary least squares (OLS) regression model (Fig. S1) was chosen to predict reaction conversion and selectivity for each candidate condition due to its low prediction error. The manipulated inputs for the reactor unit were water content (0 wt% to 20 wt%), HMF loading (1 wt% to 5 wt%), temperature (190 °C to 210 °C), H₂ pressure (0 bar to 10 bar), and reaction time (3 h to 6 h). In the second-stage (Bayesian optimization of cost and emissions), new reaction condition samples were suggested via NEXTorch, and the HMF conversion and DMF selectivity were estimated from the OLS regression model without carrying out new experiments. Next, the separation sections (Figs. 3 and S8–S10) were adjusted accordingly to meet the

product requirements and the water contents in the recycle stream. TEA and LCA were then conducted to evaluate the objective function – MSP and GWP, which provide new data to update the Gaussian process cost and emission surrogate models for the next Bayesian optimization iteration.

3. Results and discussion

3.1. Reaction metrics: product composition in initial sampling and active learning

Fig. 4 shows the overall optimization progression from the sampling (Fig. 4A) and the average DMF selectivity and HMF conversion (Fig. 4B and 4C). The average DMF selectivity and HMF conversion show significant scatter due to the stochastic nature of the LHS and the iterative nature of NEXTorch. In subsequent qEI optimization trials, the HMF conversion reaches 100% (Fig. 4C) and the DMF selectivity exceeds 70%. After the 5 trials, a DMF selectivity of 79% was reached.

Figs. 5 and 6 show that the water content negatively influences both DMF selectivity and yield; the DMF selectivity and yield peak at $\sim\!201\,$ °C, between 4.2 and 4.8 hr.

We further investigated the yield toward the furan-2-pentanol ethers (Fig. 7). At 190 °C, significant ether yield (>6%) at higher water loading and low reaction times is observed. However, at 210 °C, the ether yield dependence on time and water is negligible. Little dependence on time and temperature is observed without water. However, at 20 wt% water, the ether yield decreased as the temperature and batch time increased. At 3 h batch time, strong total ether formation at high water contents and low temperature is seen; at 6 h, insignificant dependence on temperature and water content was found. Upon inspecting the overall furan material balance based on ethers and DMF (combined ethers and DMF yield divided by HMF conversion, Figs. S4 and S5), a slight reduction of furan material balance at higher water loadings at both temperatures is seen, with lower material balance at higher temperature, a potential indication of humins formation. Ether concentration is maximized at lower temperatures and higher water concentrations, potentially because these conditions slow down the reaction progression and favor the earlier products and ethers.

3.2. Systems metrics: techno-economic analysis (TEA) and life cycle assessment (LCA) at representative reaction conditions

Fig. 8 illustrates the MSP breakdown for five representative processes (shown in Table 1). In all cases, the raw material cost is the leading

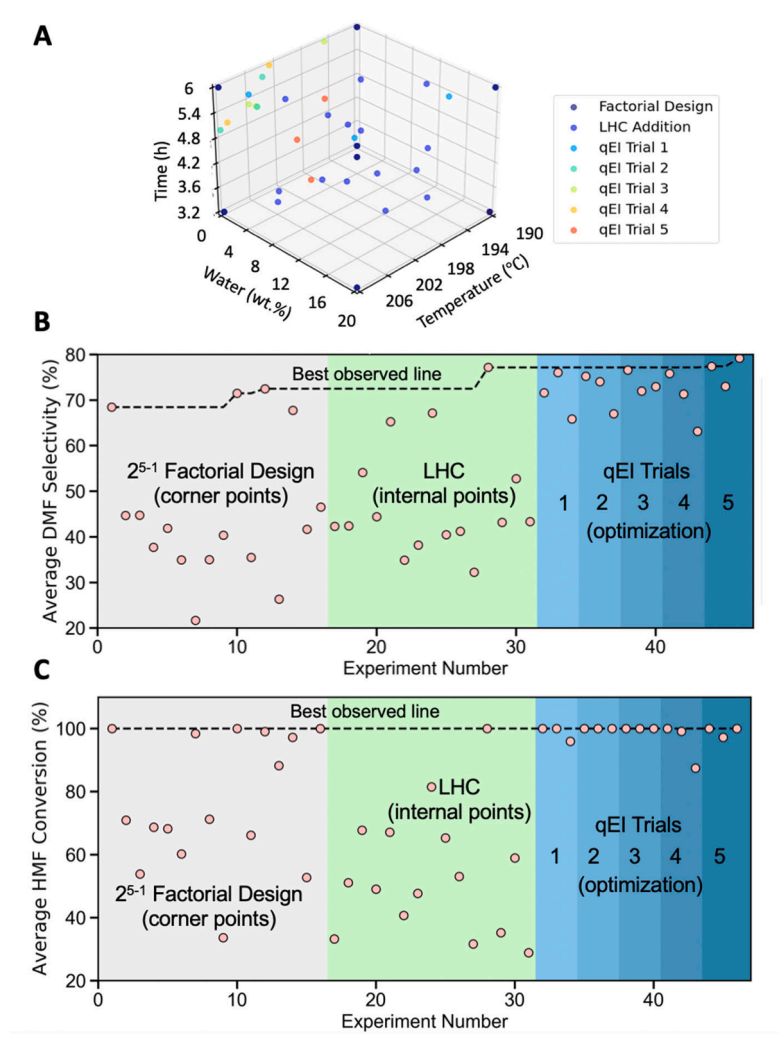


Fig. 4. Sampling point distribution and response progression. (A) Distribution of all sampling points in the design space. Only three of the five independent variables are shown; the HMF load (1–5 wt%) and hydrogen partial pressure (0–10 bar) are not shown. (B) Optimization of the DMF selectivity, spanning the factorial design (16 conditions in duplicates), Latin hypercube (15 conditions), and qEI optimization trials (5 trials of 3 conditions each). (C) Progression of the average HMF conversion throughout the optimization of DMF selectivity.

contributor to the MSP. Consequently, the production cost decreases significantly when the DMF yield increases and less humins are generated. Processes with low or no water loading (case IV and case V), with close to the optimum DMF selectivity, are among the most economically viable ones. Although the high-water content and low HMF loading scenario (case I) also give good DMF selectivity, high utility and separation unit costs make it less attractive. Low solvent cases (case II and case III) have much smaller equipment sizes and considerably lower capital costs. In all cases, pentanol solvent loss during filtration impacts the cost significantly. Thus, case III has not only the lowest pentanol loss (\$1195/t) but also the lowest MSP. Since this HDO technology is still in its early stage of development, improvements in the filtration operation and upstream HMF production will have great cost-reduction potentials. If the solvent loss during humins filtration could be eliminated, case IV and case V would have slightly lower MSP than case III. Reduction in the water content that is carried from the upstream dehydration reaction to the HDO reactor will also be beneficial.

The LCA results are shown in Fig. S14, which follow the trend of MSP. The HMF raw material and pentanol solvent are still the main emission contributors, while the steam usage in the distillation also leads to high GWP despite its low share in operating costs.

3.3. Bayesian optimization to minimize MSP and GWP

Based on the OLS regression model in Fig. S1, DMF production process flowsheets with updated reaction yields and separation requirements were generated. The MSP and GWP were calculated for each reaction condition, providing a dataset to build the Gaussian process surrogate model and keep iterating. Bayesian optimization was performed to find HDO reaction conditions that minimize the cost and greenhouse gas emissions.

As illustrated in Fig. 9A, the DMF's MSP gradually decreases from \$5420/t to \$4022/t as the iterations of Bayesian optimization continue. As shown using TEA, the HMF cost is the leading cost contributor. Hence, the MSP of DMF decreases significantly when the DMF yield increases and less humins form. This typically happens with little or no water loading, giving a high DMF selectivity. The water concentration in the last few Bayesian optimization trials is 0% or 4%, with the zerowater case having a slightly lower MSP (\$ 312/t). The optimal HMF loading of 3% balances the high solvent loss at low HMF concentration and the reduced DMF selectivity at high HMF concentration. Moreover, the best residence time is at the lowest limit of 3 h; higher residence times do not necessarily improve the DMF selectivity yet requiring larger equipment and thus a higher capital investment. The high reaction temperature (210 °C) and H₂ pressure (10 bar) result in a high HMF

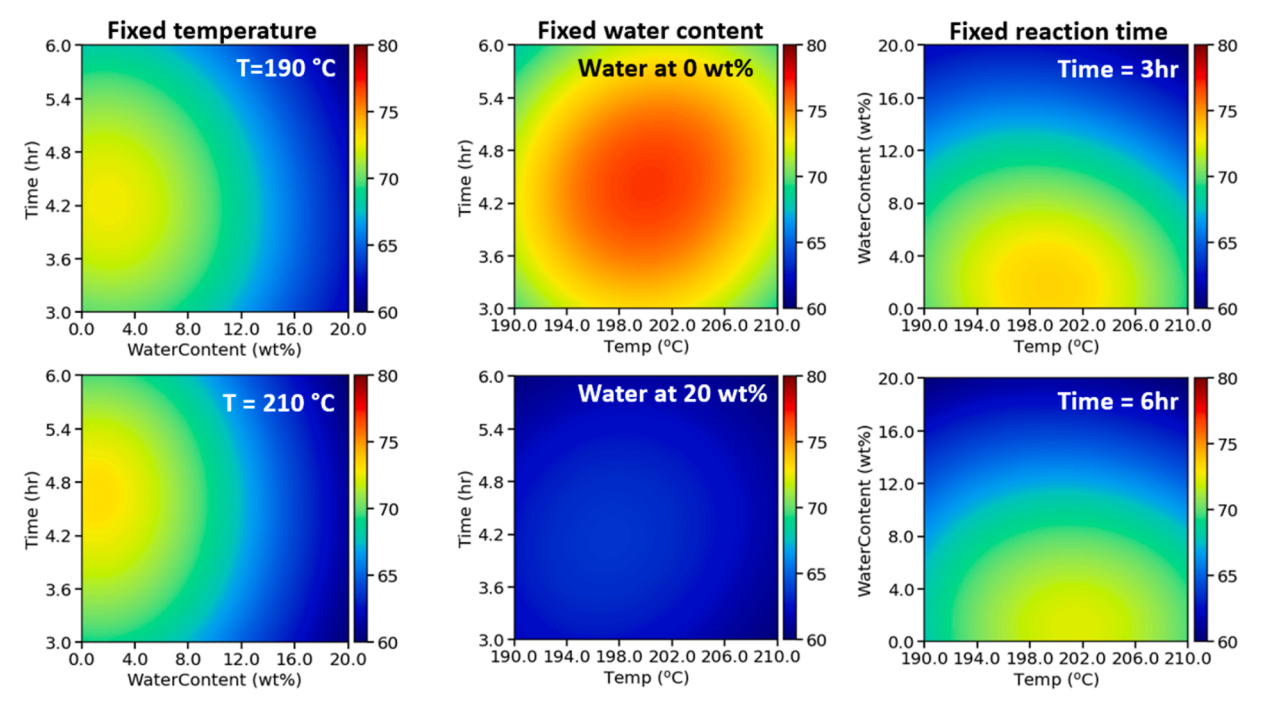


Fig. 5. DMF selectivity (%) heatmap cuts over the prescribed experimental conditions. For the heat maps, the HMF loading is 1 wt% and the hydrogen partial pressure is 10 bar.

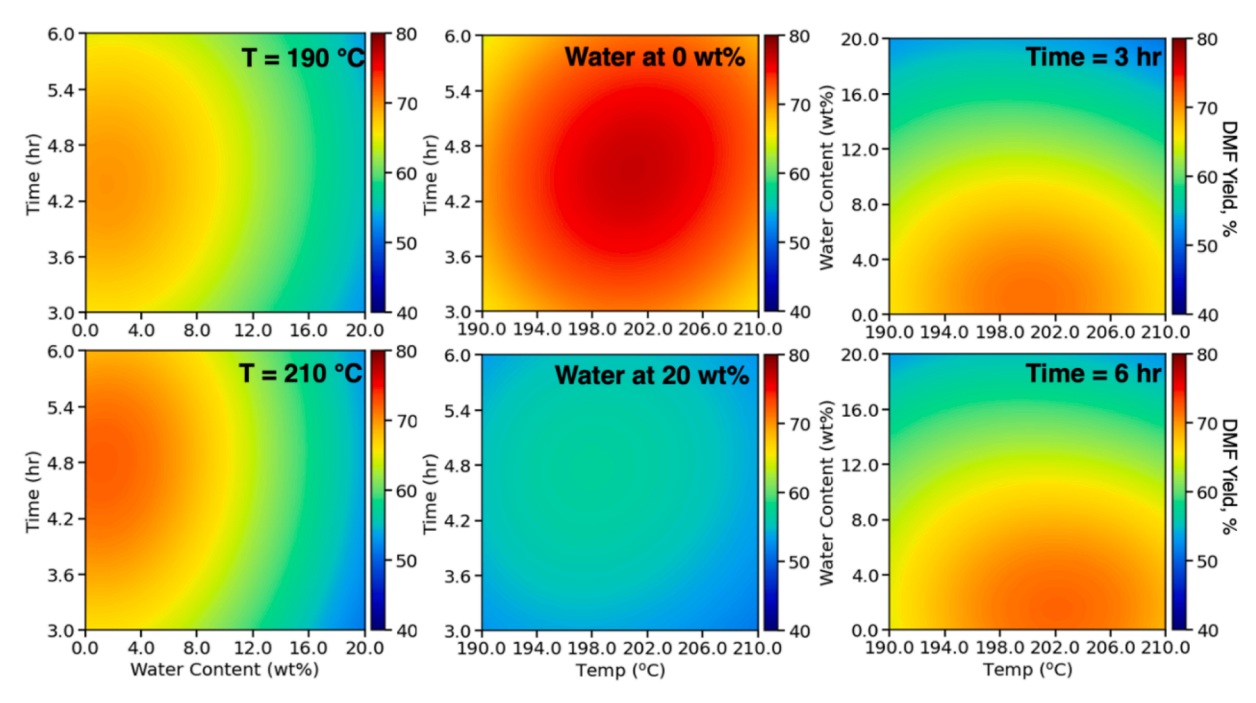


Fig. 6. DMF yield (%) heatmap cuts over the prescribed experimental conditions. For these graphs, the HMF loading is 1 wt% and the hydrogen partial pressure is

conversion at short reaction times. Although higher H_2 pressures lead to more expensive compressors and reactors, a slight drop in H_2 pressure causes a significant reduction in DMF yields and is undesirable.

The Bayesian optimization for the GWP paralleled the MSP trend (Fig. 9B), following the increase of HMF conversion and DMF selectivity. This is also confirmed by the multi-objective optimization results in NEXTorch (Fig. S13), where trade-offs of MSP and GWP exist only at very extreme points, while most points with a low MSP also have a low GWP. As raw material consumption is the leading contributor to both

cost and emissions, improving HMF conversion and DMF selectivity achieves GWP and MSP minimization goals simultaneously. Consequently, cost and greenhouse gas emission were non-competing targets for most points explored by multi-objective Bayesian optimization. High $\rm H_2$ pressure, medium HMF loading (3 wt%), and no water in the feedstock are still favored for GWP minimization. Nevertheless, the utilities to heat the inlet stream before the reaction play an essential role in the GWP. Despite minimal effects on the MSP, the HDO reaction temperature needs to be reduced from 210 $^{\circ}{\rm C}$ to 199 $^{\circ}{\rm C}$ to lower greenhouse gas

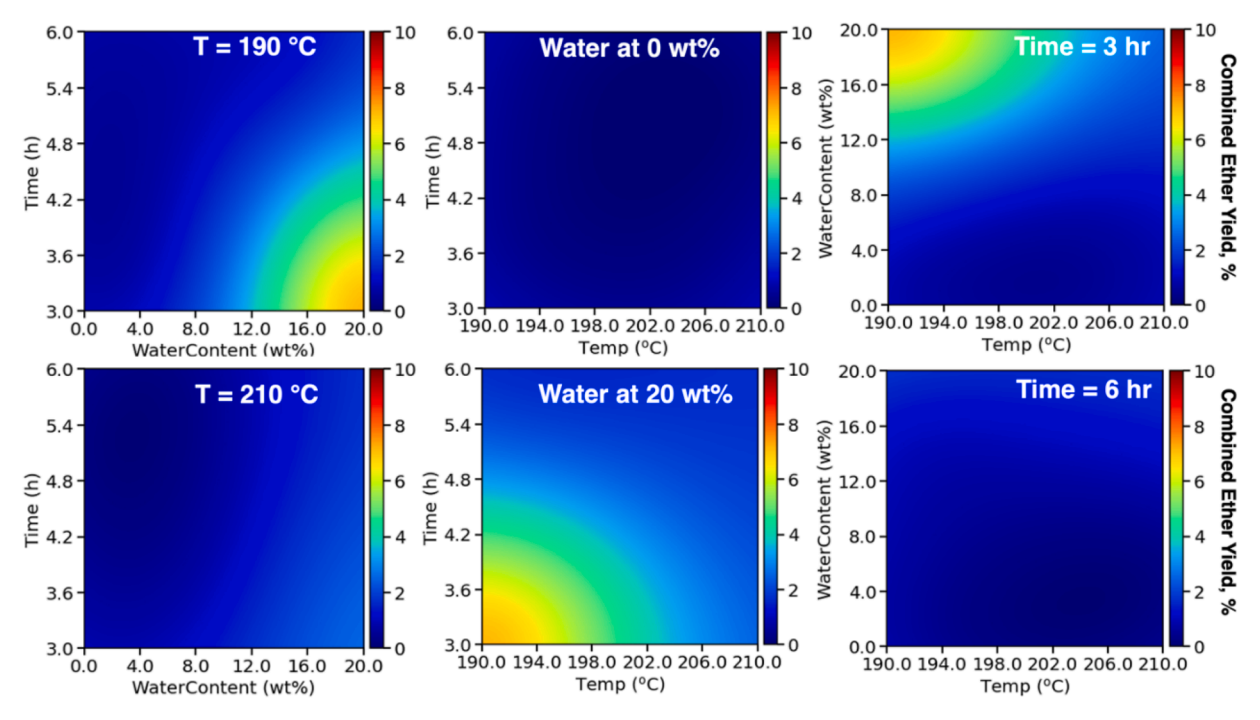


Fig. 7. Yield (%) heatmap of ethers 1–4 (combined) over the prescribed experimental conditions. The HMF loading is 1 wt% and the hydrogen partial pressure is 10 bar. For the individual furan-alcohol ethers, the heatmaps are provided in the Supplementary Material.

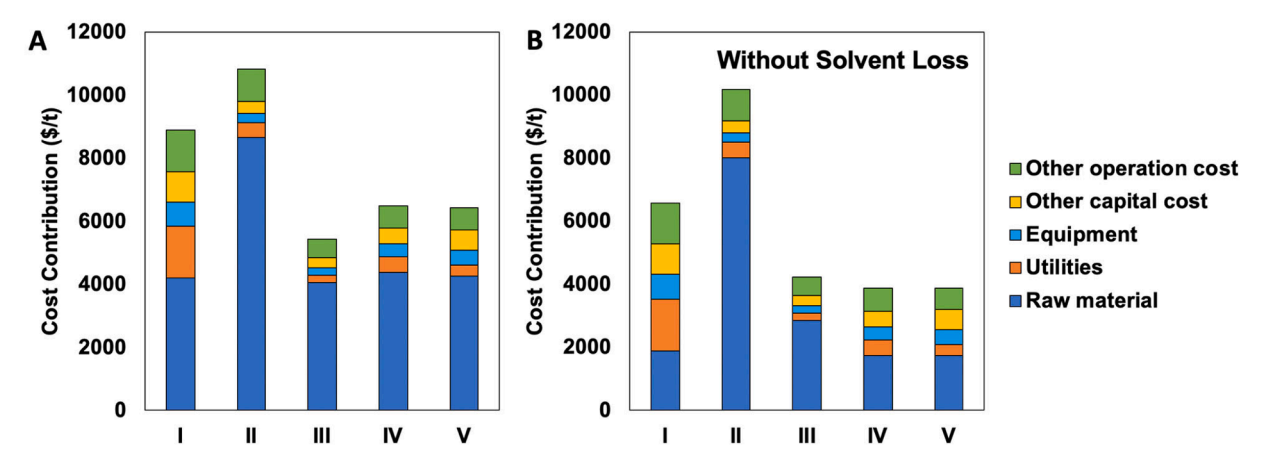


Fig. 8. Comparison of the minimum selling prices. (A) 1% solvent loss during filtration; (B) no solvent loss during filtration.

emissions, which illustrated only a slight trade-off between GWP and MSP. Based on the conversion and selectivity OLS regression model (Fig. S1), the lowest GWP is obtained with an increased reaction time from 3 h to 4.3 h to achieve good DMF yields under a lower reaction temperature. Longer reaction times result in larger reactors but impact slightly the process greenhouse gas emissions since the plant will run for many years and even serve for other purposes after its designed life (Athaley et al., 2019a, 2019b). The GWP reduces from 26.5 kg CO₂ eq/kg DMF to 22.5 kg CO_2 eq/kg DMF after the Bayesian optimization. Water in the reactant causes a drastic GWP increase since the azeotrope compositions significantly affect the distillation operating conditions, leading to high utility usage. 4 wt% water in the inlet gives a GWP of 31.1 kg CO₂ eq/kg DMF, 38.4% higher than the conditions without water. Since raw material and solvent usage are identified as the main bottlenecks of the HDO process, future improvements on the upstream HMF production and filtration technologies will most effectively cut down MSP and GWP. Moreover, heat integration could potentially further reduce greenhouse gas emissions due to high steam usage, but it will not substantially lower DMF production costs.

4. Conclusions

Reaction engineering studies typically focus on optimizing the product yield without considering the cost and emissions as ultimate metrics for plant design. In such studies, yield optimization is typically done by varying one parameter at a time or at best using a static design of experiments. The current work combined bench-top experiments, process simulation, and Bayesian optimization to optimize reaction conditions iteratively by varying many parameters at once. Our goal was to minimize the GWP and the cost (systems metrics) and correlate them with selectivity and yield (reaction engineering metrics). We applied this framework to produce DMF from HMF. We also considered small fractions of water in the feed coming from the upstream dehydration reactor to assess the impact of purity of the feed as a first attempt for process integration.

Reduction of the production cost and GWP approximately follows the $\,$

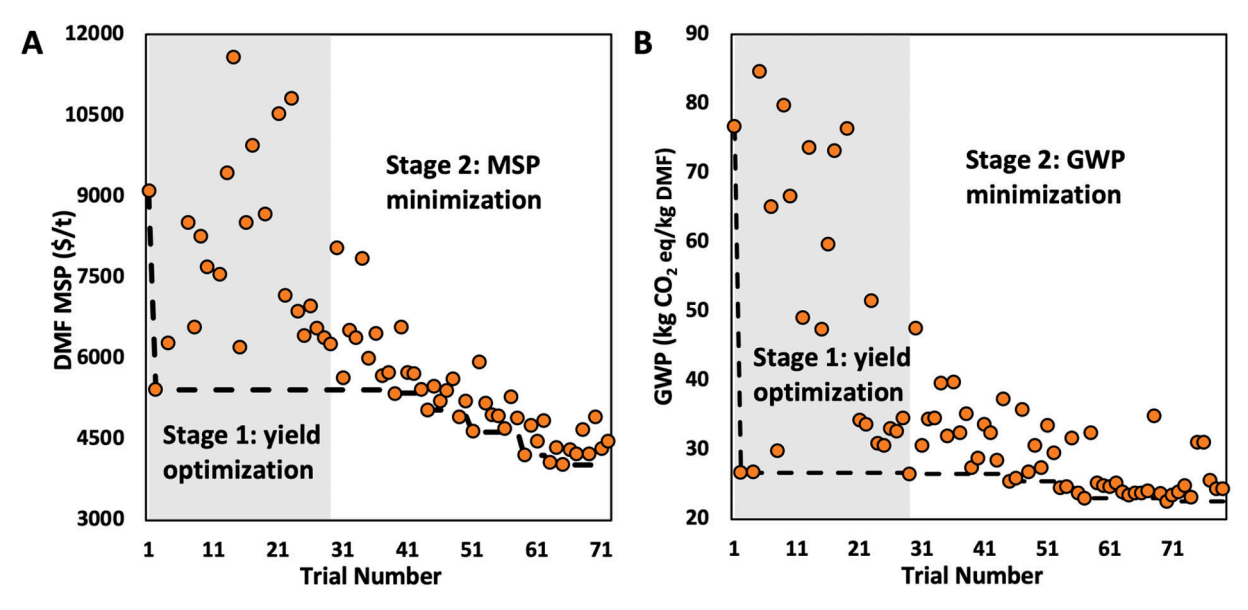


Fig. 9. Discovery plots of the process-level optimization of DMF production. (A) minimum selling price (MSP) and (B) global warming potential (GWP).

conversion and yield maximization strategy. This is a result of the dominant cost of the feed (HMF), a general characteristic of biomass processes (Athaley et al., 2019a; Luo et al., 2022). The solvent cost and any loss of the solvent (e.g., in filtration) significantly increase the DMF cost. Optimal reaction conditions favor a high hydrogen pressure, relatively high temperatures, medium HMF loadings, and no or low water, which correspond to low HMF feedstock usage, utility consumption, and solvent loss. These conditions are overlooked in the reaction optimization but selected during the systems optimization because process integration is considered to include product purification and solvent recovery steps. Interestingly, we see no significant tradeoff between GWP and MSP. A non-intuitive result is that water in the feed impacts the GWP negatively much more than its production cost.

CRediT authorship contribution statement

Zhaoxing Wang: Conceptualization, Data curation, Formal analysis, Investigation, Methodology, Writing – original draft. Yuqing Luo: Data curation, Formal analysis, Investigation, Methodology, Writing – original draft. Prahalad Srinivasan: Investigation. Yifan Wang: Resources, Software. Tai-Ying Chen: Resources, Software. Marianthi G. Ierapetritou: Conceptualization, Funding acquisition, Supervision, Writing – review & editing. Dionisios G. Vlachos: Conceptualization, Funding acquisition, Supervision, Writing – review & editing.

Declaration of competing interest

The authors declare the following financial interests/personal relationships which may be considered as potential competing interests: Zhaoxing Wang, Yuqing Luo, Prahalad Srinivasan, Yifan Wang, Tai-Ying Chen, Marianthi G. Ierapetritou, and Dionisios G. Vlachos reports financial support was provided by National Science Foundation. If there are other authors, they declare that they have no known competing financial interests or personal relationships that could have appeared to influence the work reported in this paper.

Data availability

Data will be made available on request.

Acknowledgements

This work was supported in part by the National Science Foundation under Grant No. 2134471.

Supplementary materials

Supplementary material associated with this article can be found, in the online version, at doi:10.1016/j.compchemeng.2024.108644.

References

Abrams, D.S., Prausnitz, J.M., 1975. Statistical thermodynamics of liquid mixtures: a new expression for the excess Gibbs energy of partly or completely miscible systems. AIChE J. 21, 116–128.

Akpa, B.S., D'Agostino, C., Gladden, L.F., Hindle, K., Manyar, H., McGregor, J., Li, R., Neurock, M., Sinha, N., Stitt, E.H., Weber, D., Zeitler, J.A., Rooney, D.W., 2012. Solvent effects in the hydrogenation of 2-butanone. J. Catal. 289, 30–41.

Aspen Economic Analyzer V11, 2019. Aspen Economic Analyzer, V11 ed. Aspen Technology, Inc, Burlington, MA.

Athaley, A., Annam, P., Saha, B., Ierapetritou, M., 2019a. Techno-economic and life cycle analysis of different types of hydrolysis process for the production of p-Xylene. Comput. Chem. Eng. 121, 685–695.

Athaley, A., Saha, B., Ierapetritou, M., 2019b. Biomass-based chemical production using techno-economic and life cycle analysis. AIChE J. 65, e16660.

Bare, J., 2011. TRACI 2.0: the tool for the reduction and assessment of chemical and other environmental impacts 2.0. Clean Technol. Environ. Policy 13, 687–696.

BASF. Pricing of precious metals for catalysts. In 2024.

Bozell, J.J., Petersen, G.R., 2010. Technology development for the production of biobased products from biorefinery carbohydrates-the US Department of Energy's "Top 10" revisited. Green Chem. 12, 539–554.

Chang, H., Bajaj, I., Huber, G.W., Maravelias, C.T., Dumesic, J.A., 2020. Catalytic strategy for conversion of fructose to organic dyes, polymers, and liquid fuels. Green Chem. 22, 5285–5295.

Chen, T.Y., Baker-Fales, M., Vlachos, D.G., 2020. Operation and optimization of microwave-heated continuous-flow microfluidics. Ind. Eng. Chem. Res. 59, 10418–10427.

Ebikade, E.O., Wang, Y., Samulewicz, N., Hasa, B., Vlachos, D., 2020. Active learning-driven quantitative synthesis–structure–property relations for improving performance and revealing active sites of nitrogen-doped carbon for the hydrogen evolution reaction. React. Chem. Eng. 5, 2134–2147.

Esteban, J., Vorholt, A.J., Leitner, W., 2020. An overview of the biphasic dehydration of sugars to 5-hydroxymethylfurfural and furfural: a rational selection of solvents using COSMO-RS and selection guides. Green Chem. 22, 2097–2128.

Gilcher, E.B., Chang, H., Rebarchik, M., Huber, G.W., Dumesic, J.A., 2022. Effects of water addition to isopropanol for hydrogenation of compounds derived from 5hydroxymethyl furfural over Pd, Ru, and Cu catalysts. ACS Catal. 12, 10186–10198.

Jae, J., Zheng, W., Karim, A.M., Guo, W., Lobo, R.F., Vlachos, D.G., 2014. The role of Ru and RuO2 in the catalytic transfer hydrogenation of 5-hydroxymethylfurfural for the production of 2,5-dimethylfuran. ChemCatChem 6, 848–856.

- Jae, J., Zheng, W., Lobo, R.F., Vlachos, D.G., 2013. Production of dimethylfuran from hydroxymethylfurfural through catalytic transfer hydrogenation with ruthenium supported on carbon. ChemSusChem 6, 1158–1162.
- Kazi, F.K., Patel, A.D., Serrano-Ruiz, J.C., Dumesic, J.A., Anex, R.P., 2011. Technoeconomic analysis of dimethylfuran (DMF) and hydroxymethylfurfural (HMF) production from pure fructose in catalytic processes. Chem. Eng. J. 169, 329–338.
- Kuznetsov, A., Kumar, G., Ardagh, M.A., Tsapatsis, M., Zhang, Q., Dauenhauer, P.J., 2020. On the economics and process design of renewable butadiene from biomassderived furfural. ACS Sustain. Chem. Eng. 8, 3273–3282.
- Luo, Y., Ierapetritou, M., 2020. Comparison between different hybrid life cycle assessment methodologies: a review and case study of biomass-based p-xylene production. Ind. Eng. Chem. Res. 59, 22313–22329.
- Luo, Y., Kuo, M.J., Ye, M., Lobo, R., Ierapetritou, M., 2022. Comparison of 4,4'-dimethylbiphenyl from biomass-derived furfural and oil-based resource: technoeconomic analysis and life-cycle assessment. Ind. Eng. Chem. Res. 8963—8972
- Nakagawa, Y., Tamura, M., Tomishige, K., 2013. Catalytic reduction of biomass-derived furanic compounds with hydrogen. ACS Catal. 3, 2655–2668.
- O'Dea, R.M., Pranda, P.A., Luo, Y., Amitrano, A., Ebikade, E.O., Gottlieb, E.R., Ajao, O., Benali, M., Vlachos, D.G., Ierapetritou, M., Epps III, T.H., 2022. Ambient-pressure lignin valorization to high-performance polymers by intensified reductive catalytic deconstruction. Sci. Adv. 8, eabj7523.
- Peter Lappe, D., Hofmann, T., 2011. Pentanols. Ullmann's Encyclopedia of Industrial Chemistry. Wiley.
- U.S. Geological Survey, 2016. Lime in 2016. 2016 Minerals Yearbook. U.S. Geological Survey.

- van Putten, R.J., van der Waal, J.C., de Jong, E., Rasrendra, C.B., Heeres, H.J., de Vries, J.G., 2013. Hydroxymethylfurfural, a versatile platform chemical made from renewable resources. Chem. Rev. 113, 1499–1597.
- Wang, Y., Chen, T.Y., Vlachos, D.G., 2021a. NEXTorch: a design and bayesian optimization toolkit for chemical sciences and engineering. J. Chem. Inf. Model. 61, 5312–5319.
- Wang, Z., Bhattacharyya, S., Vlachos, D.G., 2020. Solvent selection for biphasic extraction of 5-hydroxymethylfurfural via multiscale modeling and experiments. Green Chem. 22, 8699–8712.
- Wang, Z., Bhattacharyya, S., Vlachos, D.G., 2021b. Extraction of furfural and furfural/5hydroxymethylfurfural from mixed lignocellulosic biomass-derived feedstocks. ACS Sustain. Chem. Eng. 9, 7489–7498.
- Wernet, G., Bauer, C., Steubing, B., Reinhard, J., Moreno-Ruiz, E., Weidema, B., 2016. The ecoinvent database version 3 (part I): overview and methodology. Int. J. Life Cycle Assess. 21, 1218–1230.
- Wijaya, Y.P., Suh, D.J., Jae, J., 2015. Production of renewable p-xylene from 2,5-dimethylfuran via Diels-Alder cycloaddition and dehydrative aromatization reactions over silica—alumina aerogel catalysts. Catal. Commun. 70, 12–16.
- Zhang, Z.M., Li, H., 2022. Water-mediated catalytic hydrodeoxygenation of biomass. Fuel 310, 122242–122259.
- Zhao, Z., Bababrik, R., Xue, W., Li, Y., Briggs, N.M., Nguyen, D.T., Nguyen, U., Crossley, S.P., Wang, S., Wang, B., Resasco, D.E., 2019. Solvent-mediated charge separation drives alternative hydrogenation path of furanics in liquid water. Nat. Catal. 2, 431–436.
- Zheng, J., Suh, S., 2019. Strategies to reduce the global carbon footprint of plastics. Nat. Clim. Chang. 9, 374–378.